scientific reports

Check for updates

OPEN

Muscone suppresses inflammation and senescence of nucleus pulposus via p53 signalling during intervertebral disc degeneration

Ruizhe Wang[1,3], Zifan Zhang[1,3], Jinhai Xu[2,3], Ye Tian[1,3], Guoqing Wen[1], Huajian Zhong[1], Leixin Wei[1], Huiqiao Wu[1], Xiaolong Shen[1], Yu Chen[1], Peng Cao[1], Yang Liu[1], Huajiang Chen[1]✉, Chen Xu[1]✉, Wen Mo[2]✉ & Wen Yuan[1]✉

Intervertebral disc degeneration (IDD) is a major cause of chronic low back pain, the mechanism of which is still unclear. Inflammation-induced extracellular matrix metabolism (ECM) dysregulation in the nucleus pulposus (NP) and NP cell senescence are known to be the key causes of IDD. However, few drugs can reliably alleviate ECM dysregulation and NP cell senescence. Muscone, as the key natural component of musk, is a widely applied antiapoptotic and anti-inflammatory drug. We found Muscone exerts protective effects by inhibiting the expression of ECM catabolism-related genes, cell apoptosis, the cell senescence and senescence-associated secretory phenotype (SASP) in NP cells, which is the key cellular phenotype associated with IDD. We have also shown that muscone can increase the expression of ECM anabolism-related genes and the proliferation of NP cells during inflammation. High-throughput RNA sequencing indicated that muscone protects NP cells mainly by altering the phosphorylation and expression of p53. Further validation confirmed both in vivo and in vitro that muscone could regulate ECM-related genes, cell apoptosis, cell senescence and the SASP by inhibiting p53. In summary, our findings show that muscone protects against the degeneration of nucleus pulposus cells by inhibiting p53 signaling and thus may have therapeutic value for IDD.

Keywords Intervertebral disc degeneration, Nucleus pulposus, Extracellular matrix metabolism, Muscone, p53

Abbreviations

IDD	Intervertebral disc degeneration
NP	Nucleus pulposus
ECM	Extracellular matrix metabolism
cLBP	Chronic low back pain
IVD	Intervertebral disc
AF	Annulus fibrosus
CEP	Cartilage end-plates
SA-β-gal	Senescence-associated β-galactosidase
SASP	Senescence-associated secretory phenotype
MMPs	Matrix metalloproteinases
MUSE	Muscone
ADAMTSs	A disintegrin and metalloproteinase with thrombospondin motifs

Chronic low back pain (LBP) and chronic neck pain are among the most common causes of disability worldwide, as reported in the Global Burden of Disease Study 2019[1]. A recent study found that nearly 80% of adults experience these conditions in their lives; thus, they impose a heavy socioeconomic burden and reduce quality

[1]Spine Center, Department of Orthopedics, Shanghai Changzheng Hospital Affiliated to Naval Medical University, 415th Fengyang Road, Huangpu District, Shanghai 200003, China. [2]Department of Orthopaedics, Longhua Hospital, Shanghai University of Traditional Chinese Medicine, 500th Wanping South Road, Xuhui District, Shanghai 200003, China. [3]Ruizhe Wang, Zifan Zhang, Jinhai Xu and Ye Tian contributed equally to this work. ✉email: spine_chen@163.com; Chenxu8836@hotmail.com; mw2218@126.com; yuanwenspine@smmu.edu.cn

of life[2–4]. Intervertebral disc degeneration (IDD) has become a major cause of chronic LBP and chronic neck pain[5,6]; thus, increasing attention has been given to its prevention and treatment. Because molecular mechanism of IDD is unclear, few effective drugs have been developed to treat patients who do not meet the indications for surgery[7].

It consists of the central gelatinous nucleus pulposus (NP), external annulus fibrosus (AF), and sandwiched inferiorly and superiorly by the cartilage end-plates (CEPs). NP tissue is mainly composed of proteoglycans and type II collagen fibers, and NP cells are the main cells that regulate the metabolism of NP ECM to cope with spinal mechanical loading and deformation[8]. NP tissues contain an abundance of water, especially in younger individuals, with the content of water reaching nearly 88%[9]. The major pathological changes associated with IDD, i.e., loss of extracellular matrix (ECM) and senescence and apoptosis of NP cells, occur in the NP tissue of intervertebral discs[10,11]. These persistent pathological changes further compromise the function of the NP and cause instability of the spine.

Cellular senescence is a major pathological characteristic of intervertebral disc degeneration and has been the focus of relevant studies[12–18]. This process can be initiated by stimuli such as oxidative stress, telomere attrition, and proinflammatory cytokines[13]. Studies have shown that a series of signaling molecules, the most well-known of which are the p53 and pRB proteins, participate in this process[14,15]. Once senescence is initiated, cells are arrested in G1 phase of the cell cycle and exhibit a characteristic morphology and gene expression, expressing markers such as *p53*, *p21*, *p16* and senescence-associated β-galactosidase (SA-β-gal)[16,17]. In addition, this process is characterized by cell apoptosis and increased expression of catabolic factors including matrix metalloproteinases (MMPs), resulting in acquisition of the senescence-associated secretory phenotype (SASP)[18].

Musk, a high-value material acquired from the ventral glandular secretion of male musk deer, is as an important crude drug in traditional Chinese medicine[19]. For more than 2000 years, musk has been applied for to maintain energy, alleviate swelling, relieve pain and so on[20]. Contemporary medical investigations have demonstrated that musk primarily consists of macrocyclic compounds, such as muscone, as well as steroids including estradiol, amino acids, inorganic salts, and additional constituents[21]. And muscone (3-methylcyclopentadecanone, Fig. 1) has several valuable pharmaceutical effects, such as an ability to act as antidote and antiapoptotic, antioxidant and antitumor effects[22]. Recent studies[22–24] have also revealed that muscone is an anti-inflammatory agent that is especially effective for treating diseases that involve chronic inflammation. Inflammation in the NP is considered the initial trigger of IDD, indicating that muscone may be effective in treating IDD. However, the effect of muscone on IDD are still unknown.

Materials and methods

Tissue sample collection

Ethics approval, informed consent and experimental protocol was approved by the ethics committee of Shanghai Changzheng Hospital (2021SL044), and We confirm that all methods were carried out in accordance with the Declaration of Helsinki. Informed consent was provided by the patients and their relatives before harvesting intervertebral disc tissue during surgery. We also confirm that all methods relative to animal experiments were carried out in accordance with relevant guidelines and regulations. The experimental protocol was approved by the Institutional Animal Care and Use Committee of Second Military Medical University. Samples of normal intervertebral disc tissue were obtained from patients with lumbar trauma in the absence of radiological indications of degeneration, who underwent spinal fusion (Pfirrmann grade I, $n=6$, age range 30 to 55 years, mean age 44 years). MRI T-2 weighted images were acquired, and the extent of intervertebral disc degeneration (IDD) was assessed utilizing the modified Pfirrmann grading system. All specimens were prepared for the isolation of nucleus pulposus cells.

Human primary nucleus pulposus cell culture

We performed NP cell isolation using a protocol rigorously validated by single-cell RNA sequencing (scRNA-seq)[25]. The collected NP tissue specimens were washed twice with sterile PBS solution. The NP region was isolated under microscopy, then minced and digested with 2 U/mL protease in DMEM medium (Gibco, NY, USA) for 20 min at 37 °C. Treating with 0.25 mg/ml type II collagenase (Gibco, Cat. No. 17101-015) for 4 h at 37 °C to obtained NP cells from the NP tissues. The remaining cell suspension was transferred into a 40 μm cell strainer (BD Biosciences, Franklin Lakes, NJ, USA) and subjected to centrifugation at 800 g for a duration of 5 min. The NP cells were subsequently resuspended in DMEM/F12 medium supplemented with 10% fetal bovine serum (FBS) (Gibco), 100 U/mL penicillin, 100 μg/mL streptomycin, and 1% L-glutamine. The cell viability exceeded 90% as determined by the cell counting kit-8 (Dojindo, Tokyo, Japan). The cells were incubated at 37 °C in an atmosphere enriched with 5% CO_2, with the culture medium being refreshed every 3 days. Cells at the second passage were utilized for additional experimental methodologies.

An in vitro model of NP cell degeneration was developed by administering recombinant human TNF-α (Peprotech, USA) (50 ng/ml) or recombinant human IL-1β (Peprotech, USA) (25 ng/ml) to the NP cells as previously reported[26]. For the overexpression of p53, a plasmid designed for p53 overexpression supplied by OBiO Technology (Shanghai) Corp., Ltd., or SCH529074 (MedChemExpress, USA), a p53 agonist, was utilized. Muscone (3-methylcyclopentadecanone) was purchased commercially with the purity over 98.0% (HY-N0633, MedChemExpress, China).

CCK-8 cell viability assay

A CCK-8 assay kit (YEASEN, Shanghai) was used to measure cell viability. Briefly, approximately 5×10^3 NP cells were seeded into each well of a 96-well plate. After treatment with the indicated group, 10 μl of CCK8 agent was added to each well according to the manufacturer's instructions. After 1–4 h of incubation at 37 °C,

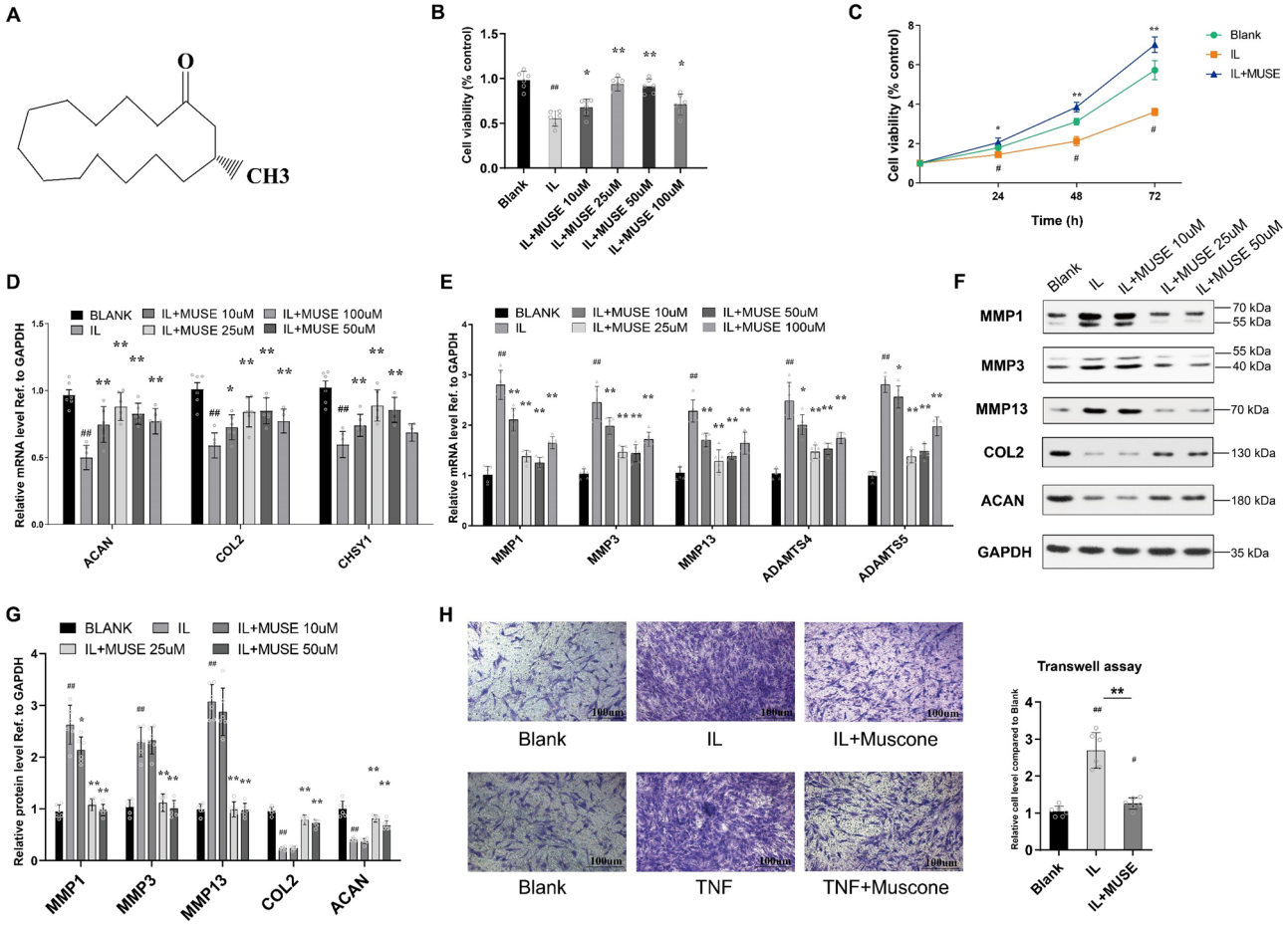

Fig. 1. Muscone shows protective effects against inflammatory irritation in NP cells. (**A**) Chem-ical structure of muscone. (**B**) CCK-8 cell viability assay of different concentrations of muscone on NP cells. (**C**) Cell proliferation assay of muscone on NP cells were measured by CCK-8. (**D**) qPCR analysis showing the relative mRNA level of ACAN, COL2 and CHSY1 expression under different concentrations of muscone treatment groups. (**E**) qPCR analysis showing the relative mRNA level of MMP1, MMP3, MMP13, ADAMTS4 and ADAMTS5 expression under different concentrations of muscone treatment groups. (**F**) The protein levels of MMP1, MMP3, MMP13, ADAMTS4, ACAN, CHSY1 and GAPDH expression in different treatment groups were assessed by Western Blot and (**G**) further quantified by comparing the gray scale to GAPDH expression. (**H**) Representative mi-croscopy images of Transwell invasion assay of NP cells in different treatment groups were shown in the left panel, migrated cells were stained with crystal purple and were calculated and shown in the right panel. Blank was used as control. All experiments were repeated at least 3 times, and GAPDH was used as an internal control for qPCR. Data are shown as mean ± SD. ##, $P < 0.01$.*, $P < 0.05$; **, $P < 0.01$. ##represented vs. Blank group, **represented vs. IL-1β treatment group.

the absorbances of different groups NP cells were measured with a multifunctional detection instrument (SPECTRAMAX 13X, Molecular Devices, USA).

TUNEL staining

Cell apoptosis was measured by transferase dUTP nick-end labeling (TUNEL) staining. Briefly, after different treatments, NP cells were fixed with 4% paraformaldehyde for 1 h and then cultured with 0.5% Triton X-100 in PBS for 10 min. After washing with PBS, the cells were incubated with reagents from a TUNEL Apoptosis Detection Kit (YEASEN, Shanghai) according to the kit's instructions for staining. The nuclear counterstaining procedure was performed by incubating samples with 0.1 mg/mL 4',6-diamidino-2-phenylindole (DAPI; Beyotime Biotechnology, Cat. No. C1002) in phosphate-buffered saline (PBS) for 5 min at room temperature. Apoptosis was observed under a fluorescence microscope (CKX41, Olympus, Japan), and photographs were obtained. At least five different fields in one sample was photographed to compare the effect.

Isolation of RNA and quantitative real-time polymerase chain reaction

RNA was isolated from human NP cells utilizing RNAiSO reagent (TAKARA, Japan) in strict adherence to the manufacturer's protocol. Quantification of total RNA concentrations was conducted at a wavelength of 260 nm using a spectrophotometer (DU-800; Beckman Coulter, Brea, CA). Reverse transcription was performed by

the PrimeScript™ RT reagent Kit with gDNA Eraser (TAKARA, Japan) in a 20-μl mixture according to the manufacturer's instructions. TB Green® Premix Ex Taq™ (TAKARA, Japan) was used to conduct real-time PCR on a Step One Plus real-time PCR system (Applied Biosystems, Foster City, CA). GAPDH was used to normalize the mRNA expression of other genes. The comparative Ct method was used to calculate the relative expression of each transcript. Each experiment was repeated at least three times independently. The primers used in this study are listed in Supplementary Table S1.

Western blotting

Ice-cold lysis buffer (Cell Signaling Technology, Danvers, MA, USA) was used to harvest total protein from human NP cells. For measurement of phosphorylated protein levels, total protein was extracted at 12–24 h after treatment. A bicinchoninic acid protein assay kit (Pierce Biotechnology, Rockford, IL, USA) was used to determine the concentration of protein. Protein degeneration was prevented by using PMSF (Beyotime, China) and protease inhibitor cocktail (Meilune, China). The proteins were subjected to transfer onto PVDF membranes (Bio-Rad, CA) via electroblotting. Subsequent to this, the membranes were blocked utilizing 5% non-fat milk in TBST (50 mM Tris (pH 7.6), 150 mM NaCl, 0.1% Tween-20) and subsequently incubated in TBST containing specific antibodies overnight at 4 °C. The protein bands were visualized using SuperSignal™ West Femto Maximum Sensitivity Substrate (Thermo Fisher Scientific, USA) and Pierce™ ECL Western Blotting Substrate (Thermo Fisher Scientific, USA) to assess the expression of target proteins. The following antibodies were used: anti-MMP1 (ab52631, 1:2500 dilution), anti-MMP3 (ab53015, 1:1000 dilution), anti-MMP13 (ab39012, 1:1000 dilution), anti-ADAMTS4 (ab185722, 1:500 dilution), anti-ADAMTS5 (ab 41037, 1:250 dilution), anti-ACAN (ab3778, 1:500 dilution), anti-CHSY1 (ab153813, 1:500 dilution), anti-p53 (ab 32389, 1:10000 dilution), anti-p-p53 (ab33889, 1:1000 dilution), anti-PUMA (ab54288, 1:1000 dilution), anti-Bax (ab32503, 1:1000 dilution), anti-p21 (ab109520, 1:1000 dilution), anti-p16 (ab 108349, 1:2000 dilution), anti-CCNG2 (ab 203314, 1:500 dilution) (all from Abcam, USA) and anti-GAPDH (1:5000 dilution) (Proteintech, USA). Uncropped images were provided in supplementary Fig. 1 (Figure S1).

High-throughput RNA sequencing and bioinformatics analysis

Total RNA was isolated for the purpose of transcriptome sequencing utilizing the TRIzol reagent (Invitrogen, Carlsbad, USA), adhering strictly to the manufacturer's prescribed protocol. Subsequently, the procedures encompassing library construction, RNA quality assurance, purification, quantification, and validation were executed by Shanghai NovelBio Bio-Pharm Technology Co., Ltd. For the analysis of the transcriptomic data, approximately 100 bp reads were aligned to the human genome (hg19) employing TopHat2/Bowtie2. The data were subsequently mapped to gene structures derived from RefSeq utilizing the summarize overlaps function in Intersect Strict mode (Genomic Ranges, Bioconductor). From the raw count data, reads per kilobase per million reads mapped (RPKM) values were computed for the identical gene set using Cufflinks. Differential expression analysis was conducted with the aid of edgeR, employing TMM (trimmed mean of M-values) library normalization and maintaining a false discovery rate (FDR) of 0.05. The datasets generated during the current study are available in the Gene Expression Omnibus (GEO) repository (GSE113633, Supplementary Dataset S1-3).

Gene Ontology (GO) and KEGG pathway analyses were performed as previously described[19]. In summary, the p value for each Gene Ontology (GO) term was calculated employing right-sided hypergeometric tests, and the Benjamini–Hochberg method was applied for the correction of multiple tests. An adjusted p value lower than 0.05 was considered indicative of a statistically significant deviation from the anticipated distribution, suggesting enrichment of the specific GO term or pathway among the target genes. We performed GO and KEGG pathway analyses of all the differentially expressed mRNAs and GO analysis of the mRNAs that were included in the miRNA regulatory network (Supplementary Dataset S2, S3).

Transwell invasion assay

An invasion assay was performed with a Matrigel-coated Transwell plate to assess MMP secretion from NP cells and the migration ability of NP cells after different treatments. NP cells were plated into the upper chamber, which was coated with Matrigel (BD Biosciences, Franklin Lakes, NJ, USA). According to our previous study[27]the inflammatory cytokines IL-1β and TNF-α were administered 8 h post-plating at concentrations of 25 ng/ml and 50 ng/ml, respectively. After an incubation period of 48 h, cells were carefully removed from the Matrigel-coated surface of the upper chamber using swabs. The invaded cells on the lower surface of the chamber were fixed with 4% paraformaldehyde for a duration of 30 min followed by staining with 0.1% crystal violet for 10 min. Distilled deionized water was employed to wash the cells until clarity of the water was achieved. The samples were then allowed to air dry before being subjected to microscopic observation. Finally, the number of invaded cells were observed and counted using a microscope by selecting five different fields from one sample to generated the average cells.

Flow cytometry

Apoptotic cell measurement was conducted through flow cytometry employing an Annexin V-FITC/PI Double Staining Kit for Apoptotic Cells (BD Bioscience, USA). Cells were harvested after a 48-hour treatment period, enzymatically digested using trypsinase without EDTA, and rinsed with PBS before being processed according to the manufacturer's protocol. Concisely, cells were resuspended in 100 μl of binding buffer, placed into a centrifuge tube, and incubated with 5 μl of dye under dark conditions for 15 min. Subsequently, 400 μl of binding buffer was added, and the samples were subjected to analysis by flow cytometry (CyAn ADP, Beckman, USA).

Cell cycle analysis
Cell cycle distribution was determined by flow cytometry using Cell Cycle Staining Kit (MultiSciences, Hangzhou). The NP cells were collected after 48 h of treatment, harvested by trypsinase without EDTA, washed by PBS, and followed up with the manufacturer's instruction. Next, 1 ml DNA Staining solution and 10 µl Permeabilization solution were added to each tube, then incubate in dark for 30 min. Then the tube was detected by flow cytometry (CyAn ADP, BECKMAN, USA).

Senescence-associated β-galactosidase (SA-β-gal) staining
A senescence β-galactosidase staining kit (Beyotime Biotechnology, Shanghai) was used to determine the percentage of SA-β-gal-positive cells. Briefly, NP cells were cultured in 6-well plates and treated for 48 h. After fixation for 15 min, the cells were washed with PBS and then incubated with staining solution overnight. Then, the staining was observed and photographed under a fluorescence microscope (CKX31, OLYMPUS, Japan). Within each well, 500 cells were analyzed to determine the percentage of SA-β-gal-positive cells.

Animal study
Male C57BL/6 mice were purchased from Shanghai Model Organisms Center, Inc. (Shanghai, China). An anterior disc puncture-induced IDD animal model was established as described in our previous study[27]. Initially, ketamine (100 mg/kg) and acepromazine(3 mg/kg) was administered via intraperitoneal injections to induce general anesthesia, and local anesthesia was done by using bupivacaine prior to the incision procedure. The mice were systematically allocated into four distinct groups: the sham surgery group, the needle puncture group, the needle puncture combined with vehicle (1:2 PBS and 1:2 DMSO) injection group, and the needle puncture combined with muscone injection group. The ventral aspect of the intervertebral disc (IVD) was accessed through an abdominal incision. A needle was vertically introduced into the disc from the ventral side and rotated 180 degrees along its axis for a duration of 10 s. A 31-gauge needle was precisely inserted 1.5 mm parallel to the endplate, traversing the annulus fibrosus (AF) to the nucleus pulposus (NP), thereby compromising the integrity of the nucleus. In the control NC injection group, a vector of 10 µl was meticulously injected into the punctured IVD, after leaving the needle in place for five seconds, the needle was carefully removed without excessive mechanical injury. In the muscone injection group, an injection of 10ul MUSE (25 µm), with or without the addition of SCH529074 (2 µm). Magnetic resonance imaging (MRI) was conducted at intervals of 0, 3, and 9 weeks subsequent to the initial surgery. The spine of mice was analyzed in sagittal T2-weighted images using a 3.0 T clinical magnet (Philips Intera Achieva 3.0 MR). T2-weighted sections in the sagittal plane were obtained using the following settings: a fast spin echo sequence with a time to repetition (TR) of 5400 ms and a time to echo (TE) of 920 ms; a 320 (h) x 9256 (v) matrix; a field of view of 260; and 4 excitations[28,29]. The section thickness was 2 mm with a 0-mm gap[28]. The Pfirrmann grading system facilitated the evaluation of intervertebral disc (IVD) degeneration. ImageJ and Surgimap software were employed to examine the alterations in the IVD[30].

Histopathological analysis and immunohistochemical staining
IVD sections from each group were subjected to hematoxylin and eosin (HE) staining and Safranin O-fast green (SO) staining. A histopathological grading system considering the cellularity and morphology of the AF and NP as well as the border between the two structures was used to evaluate histopathological changes[31]. A histopathological score of 5 indicated no degeneration, 6–10 indicated moderate degeneration and 11–15 indicated severe degeneration. Briefly, the sections were blocked with 1% (w/v) goat serum albumin at 37 °C for 1 h. Then, the sections were incubated with primary antibodies (p53, p16, p21; 1:100 dilution) overnight at 4 °C, followed by incubation with HRP-conjugated secondary antibodies for 1 h at 37 °C. The samples were imaged by a Zeiss microscope (Zeiss Axio Imager A2, Carl Zeiss Microscopy GmbH, Jena, Germany).

Statistical analysis
The data are presented as the mean ± standard deviation of at least three independent experiments. GraphPad Prism 6.0 software (GraphPad Software, Inc., San Diego, CA, USA) was used for statistical analysis. The normality of the data was tested using the D'Agostino-Pearson omnibus normality test. The proportion of immune-positive NP cells in human NP tissues failed to satisfy the normality test; consequently, these data were subjected to analysis using the two-tailed Mann–Whitney U test. Conversely, the remaining datasets met the criteria for normality and were accordingly analyzed using the two-tailed Student's t-test for the comparison between two groups, or through analysis of variance (ANOVA) followed by Tukey's t-test for multiple group comparisons. The threshold for significance was established at 0.05.

Results
Muscone inhibits the decrease in NP cell viability triggered by IL-1β
To explore the effect of muscone (Fig. 1A) on NP cells in the presence of IL-1β, NP cells were treated with different concentrations of muscone, including 10, 25, 50 and 100 µM. As shown in Fig. 1B, cell viability was significantly decreased in the IL-1β treatment group compared with the blank group. In the 10 µM muscone group, cell viability was only slightly increased compared to the IL-1β treatment group ($P<0.05$), while 25 µM and 50 µM muscone-treated NP cells showed an obvious increase in viability ($P<0.01$). However, in the 100 µM muscone group, cell viability was only slightly increased compared to that in the IL-1β treatment group ($P<0.05$), indicating an overdose effect at 100 µM. Thus, 25 µM muscone was selected as the optimum concentration for the following experiments.

To further explore the impact of muscone on NP cell viability in the presence of IL-1β, we assessed cell proliferation using the CCK-8 assay. The results demonstrated that 25 µM muscone obviously increased cell proliferation in the presence of IL-1β ($P<0.01$, Fig. 1C).

The dysregulation of ECM-related genes in NP cells caused by IL-1β can be ameliorated by muscone

To study the effect of muscone on ECM metabolism in the NP, we measured the expression of anabolism- and catabolism-related ECM genes in the NP by quantitative polymerase chain reaction (qPCR). We found that the decreased mRNA expression of *ACAN*, *COL2* and *CHSY1* in degenerated NP cells stimulated with IL-1β was significantly inhibited in the 25 μm and 50 μm muscone group ($P<0.01$), Furthermore, 10 μm muscone sightly reversed the degeneration phenotype of IL-1β ($P<0.05$), however, 100 μm muscone has no significantly effect on CHSY1 ($P>0.05$) (Fig. 1D). On the other hand, the expression of catabolism-related genes such as *MMPs* and *ADAMTS* decreased significantly after 25 μm and 50 μm muscone treatment ($P<0.01$) (Fig. 1E). Similar results were found for the protein expression of anabolism- and catabolism-related genes by Western blotting ($P<0.01$) (Fig. 1F and G). As expected, 25 μM muscone showed a stronger effect than the other concentrations.

Inflammatory cytokines can induce the degeneration of NP cells by increasing the expression of catabolism-related ECM genes, such as *MMPs* and *ADAMTS*; thus, we performed an invasion assay with a Matrigel-coated Transwell plate to further test the effect of muscone on the production of catabolism-related ECM factors in degenerated NP cells stimulated by IL-1β. Migrated NP cells were observed in the inflammatory cytokine groups, indicating that the expression of catabolism-related ECM genes was significantly increased and that these genes digested the Matrigel, allowing the migration of NP cells ($P<0.01$) (Fig. 1H). However, fewer migrated cells were observed in the muscone groups than in the other groups, indicating that muscone apparently reduced the production of catabolism-related ECM genes (Fig. 1G).

Muscone alleviates the apoptosis of NP cells induced by inflammatory factors

Considering that muscone is one of the validated anti-apoptotic agents, its effect on cell apoptosis was also tested. We performed flow cytometry and TUNEL staining on NP cells under different conditions to determine the effect of muscone on inflammatory cytokine-induced cell apoptosis. We found that the inflammatory factors IL-1β ($P<0.01$) and TNF-α ($P<0.01$) both markedly elevated the percentage of apoptotic NP cells, and the addition of muscone ($P<0.01$) decreased the percentage of apoptotic NP cells, as determined Annexin V-FITC/PI double staining and flow cytometry, however, in TNF-α group, muscone sightly decreased the early apoptosis cells ($P<0.05$)(Fig. 2A-D). As expected, TUNEL staining showed similar results: the number of apoptotic cells was significantly increased after IL-1β or TNF-α treatment, and this change was markedly reversed by muscone (Fig. 2E and F). Cell cycle analysis was also conducted, and similarly, the results showed fewer G2 phase NP cells after treatment with IL-1β for 48 h, but muscone significantly accelerated cell cycle progression ($P<0.01$) (Fig. 2G-J).

Muscone alleviates cell senescence and acquisition of the SASP in degenerated NP cells

To determine the effect of muscone on NP cell senescence in vitro, we treated NP cells with IL-1β with or without muscone and analyzed the levels of cell senescence and SASP markers. The expression of the SASP markers MMP3, MMP13, IL-6 and IL-8 was significantly elevated at both the protein and mRNA levels in IL-1β-treated NP cells, as determined by qPCR and Western blotting, whereas muscone treatment decreased the expression of these SASP markers significantly ($P<0.01$) (Fig. 3A–C). qPCR demonstrated that the expression of the cell senescence markers $p16^{INK4A}$ and $p21^{CIP}$ [32] was markedly increased in IL-1β-treated NP cells, while 25 μm muscone treatment reversed this effect ($P<0.01$), but 50 μm muscone has no significantly effect on the mRNA of $p21^{CIP}$ ($P>0.05$) (Fig. 3D). These results were also confirmed by Western blot analysis and further quantification of the results ($P<0.01$) (Fig. 3E,F). Using SA-β-gal staining, we confirmed the senescence phenotype of NP cells after IL-1β treatment, as SA-β-gal staining was increased; however, 25 μm muscone treatment remarkably reversed the increase in the number of NP cells with a senescence phenotype ($P<0.01$), 50 μm muscone provided sightly effect ($P<0.05$) (Fig. 3G,H). Taken together, these results showed that 25 μM muscone showed a stronger effect than the other concentrations.

p53 is a downstream target of muscone in degenerated NP cells

To elucidate the mechanism underlying the effect of muscone in NP cells, we conducted RNA sequencing to explore the downstream targets of muscone. Hierarchical clustering showed differential gene expression after muscone treatment (Fig. 4A). Compared with IL-1β treatment, the muscone treatment group showed 1666 differentially expressed genes, including 693 upregulated genes and 973 downregulated genes (Fig. 4B,C). To further investigate the involved pathways, we performed KEGG pathway analysis (Fig. 4D). PI3K-Akt signaling and p53 signaling were found to be significantly enriched for the differentially expressed genes. Further analysis of the sequencing data showed that *p53*, *BCL2* and *CDKN1A* are involved in both of these signaling pathways, and in vitro validation showed that the expression of p53 was obviously reduced after muscone treatment compared with after IL-1β treatment alone ($P<0.01$) (Fig. 4E); thus, we assumed that p53 signaling may be more important than *BCL2* and *CDKN1A* signaling for the function of muscone. We evaluated the expression changes in critical p53 signaling pathway factors and showed that only p53 expression was significantly affected by muscone treatment in NP cells ($P<0.01$,) (Fig. 4F).

Muscone attenuates the degeneration, senescence and apoptosis of NP cells via p53 signaling

Next, to further investigate the role of p53 signaling in protective effect of muscone against NP cell degeneration, we first induced overexpression of p53 in NP cells. The qPCR results showed that p53 overexpression markedly reversed the upregulation of anabolism-related ECM genes in the NP ($P<0.01$) (Fig. 5A) and reversed the downregulation of anabolism-related ECM genes in the NP by muscone ($P<0.01$) (Fig. 5C). Furthermore, we used SCH529074, a known p53 agonist[33]to activate p53 and found that p53 activation could remarkably

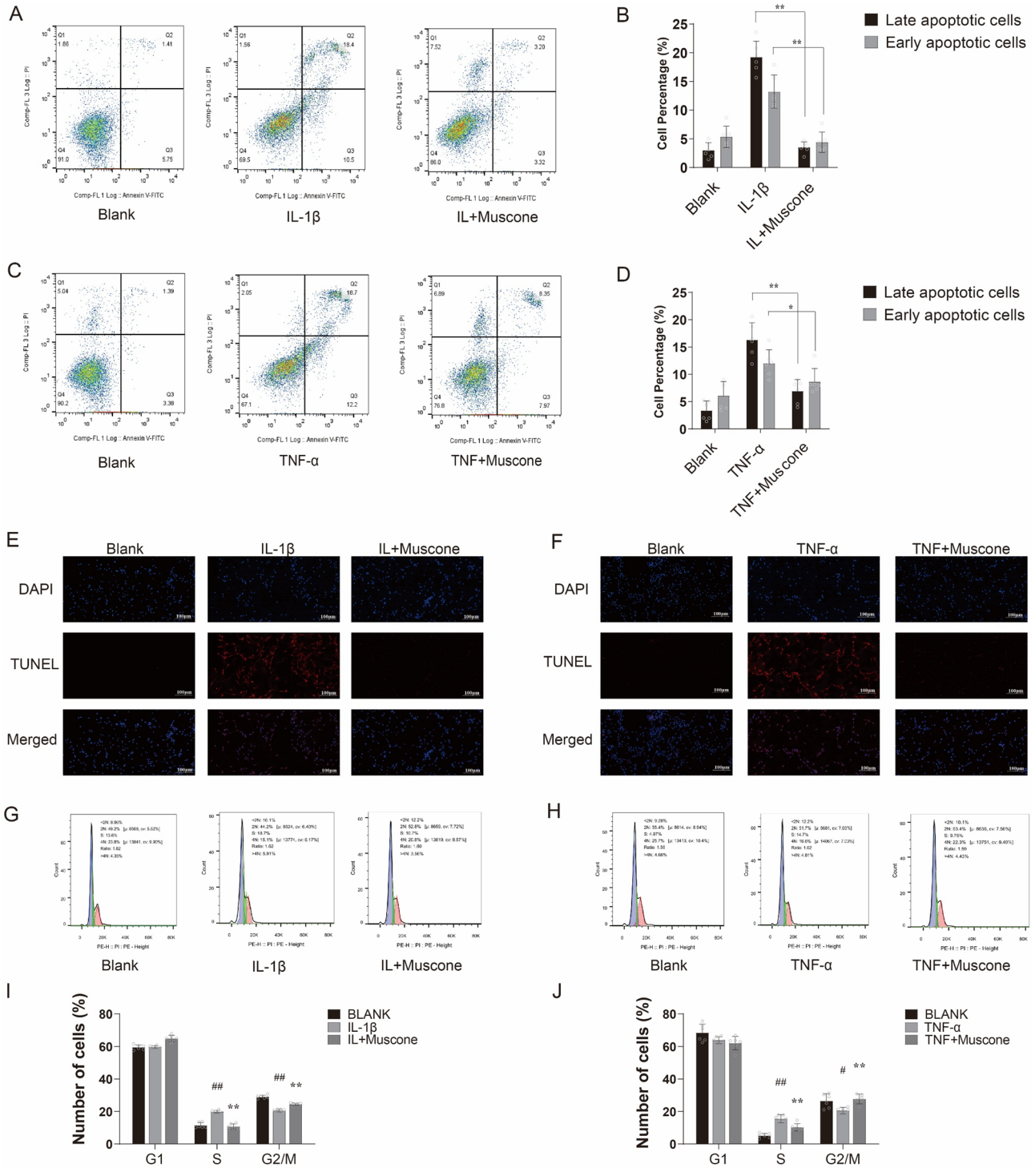

Fig. 2. Muscone alleviates the cell apoptosis and impaired cell cycle of NP cells induced by IL-1β. (**A**) Annexin V-FITC/PI Double-staining apoptosis assay showing the percentage of apoptotic percentage of NP cell under IL-1β and IL-1β + muscone treatment. (**B**) The mean percentage of early apoptotic cells and late apoptotic cells in each group was shown in the right panel. (**C**) The cell apoptosis of NP cells under TNF-α and TNF-α + muscone treatment was measured by flow cytom-etry. (**D**) The mean percentage of early apoptotic cells and late apoptotic cells in each group was shown in the right panel. TUNEL assay was used to measure cell apoptosis of NP cells under IL-1β (**E**) and TNF-α (**F**) treatment, bar represents 100 μm. The flow cytometry showing the cell cycle of NP cells under IL-1β (**G**) and TNF-α (**H**) treatment. The number of cells in different cell cycle under IL-1β (**I**) and TNF-α (**J**) treatment were shown in the panel. All experiments were repeated 3 times. Data are shown as mean ± SD. *, $P < 0.05$; **, $P < 0.01$.

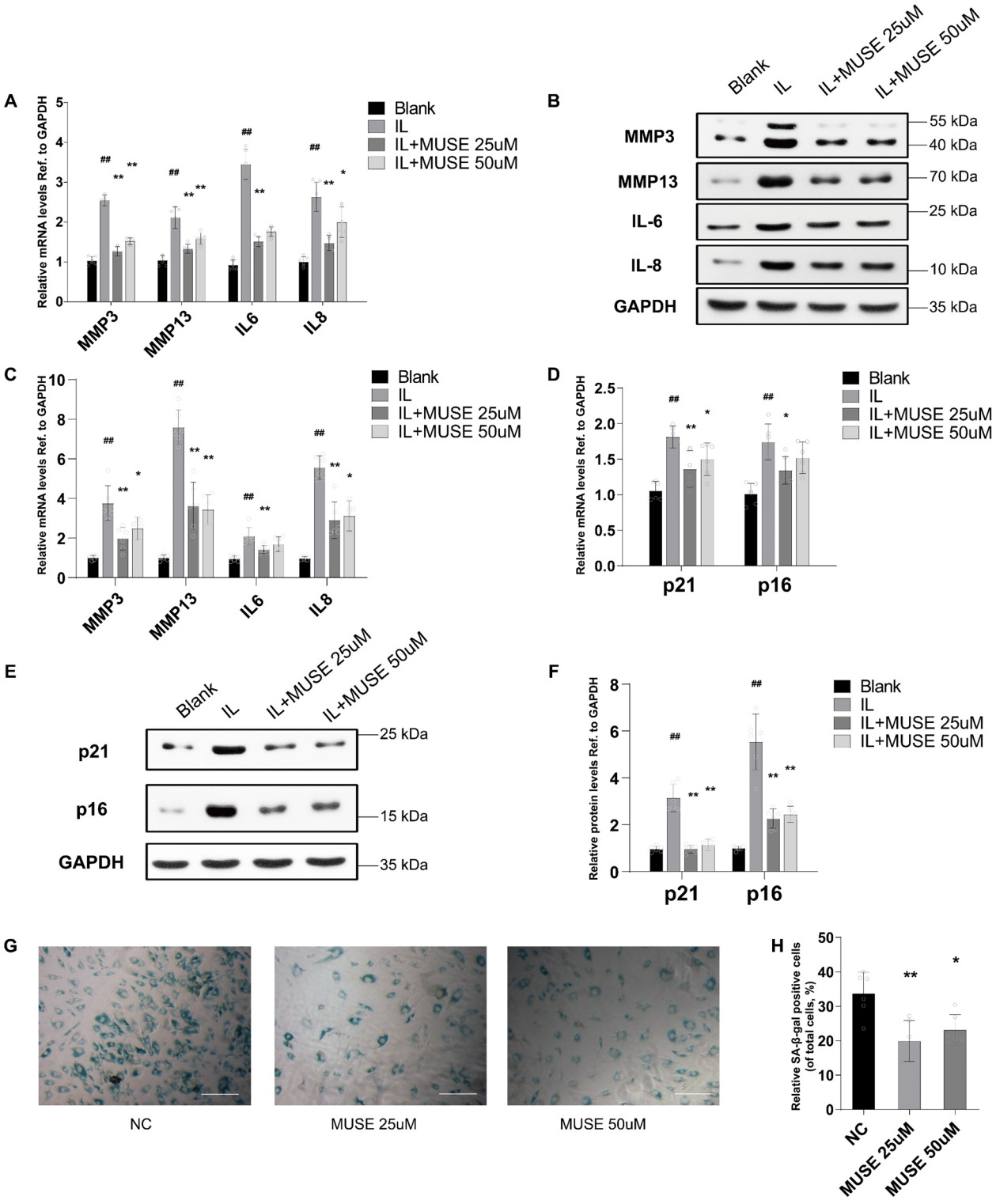

Fig. 3. The effect of muscone on cell senescence and SASP phenotype in degenerated NP cells. (**A**) qPCR analysis showing the relative mRNA expression level of SASP factors MMP13, MMP3, IL-6 and IL-8 in the NP cells under different treatment. (**B**) Western Blot analysis showing the protein level changes of SASP factors in each group, relative quantification was shown in (**C**). (**D**) The relative mRNA level of p16INK4A and p21CIP expression detected by qPCR in the NP cells. (**E**) Western Blot analysis showing the protein levels of p16INK4A and p21CIP in each group, relative quantification was shown in (**F**). (**G**) SA-b-gal staining was detected, and positive cells were quantified, bar represents 200 μm (**H**). All experiments were repeated at least 3 times, and GAPDH is used as an internal control. Data are shown as mean ± SD. #$P < 0.05$; ##, $P < 0.01$.*, $P < 0.05$; **, $P < 0.01$. ##represented vs. Blank group, **represented vs. IL group.

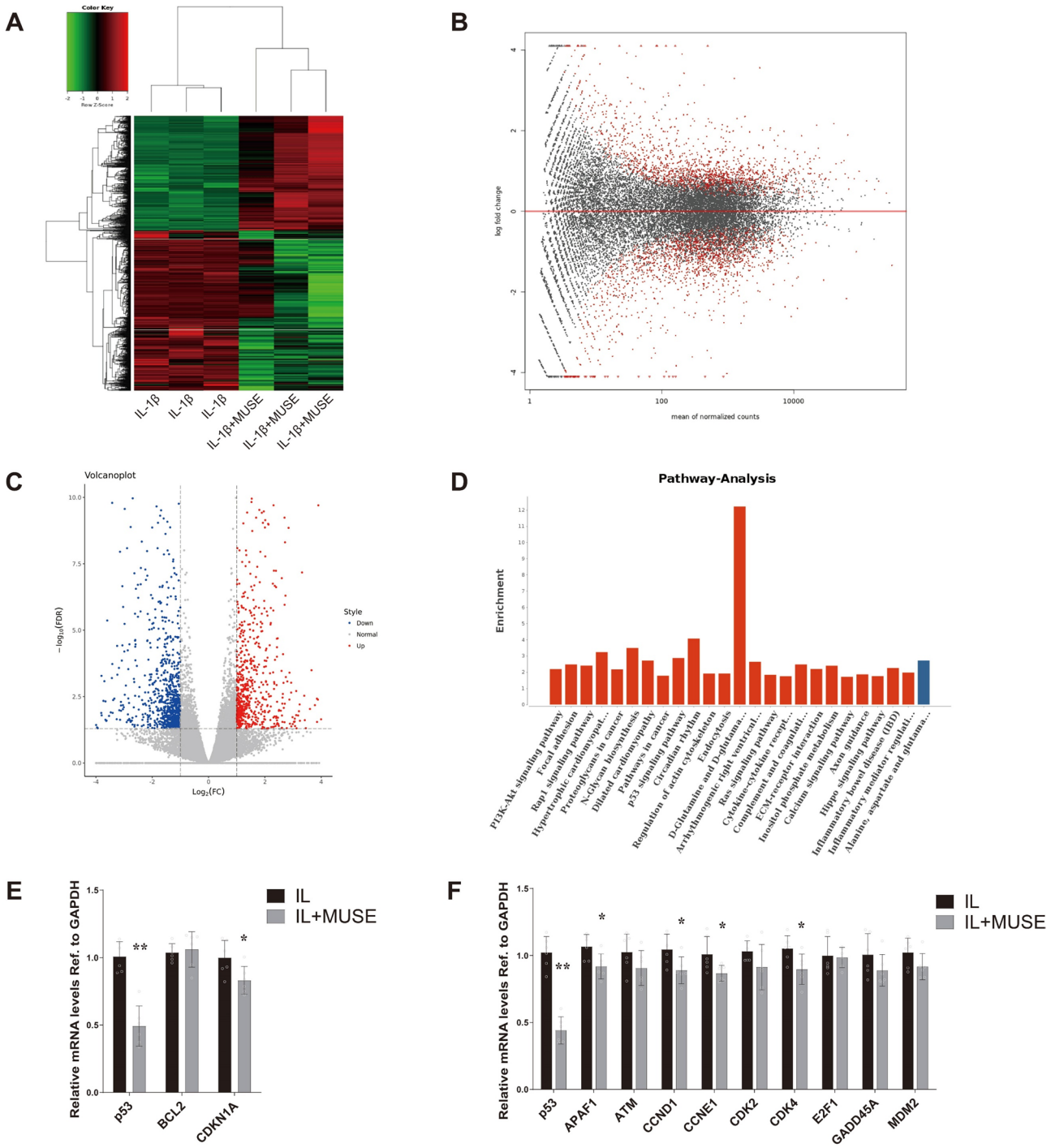

Fig. 4. High through-put RNA sequencing showing p53 the main target of muscone. (**A**) RNA-seq was used to detect the differential expressed genes of muscone treatment degenerated NP cells in IL-1β environment, the heatmap of unsupervised hierarchical cluster analysis showing the differentially expressed genes in muscone treated dataset. Each row represents the relative expres-sion level of each gene in different samples. The MA plot (**B**) and the volcano plot (**C**) showing the significantly differentially expressed genes between muscone treatment and non-treated degener-ated NP cells induced by IL-1β. (**D**) The KEGG pathway enrichment analysis showing the most abundant GO terms in the muscone treated NP cell dataset, note that the p53 signaling pathway is significantly enriched (red bars, FDR < 0.05, $P < 0.05$). qPCR analysis showing the relative mRNA expression levels of the candidate muscone target gene (**E**) or related pathway gene (**F**). The qPCR experiments were repeated 3 times, and GAPDH is used as an internal control. Data are shown as mean ± SD. *, $P < 0.05$; **, $P < 0.01$.

rescue the changes induced by muscone ($P<0.01$) (Fig. 5B,D). Western blotting confirmed these findings at the protein level ($P<0.01$) (Fig. 5E,F). We also performed an invasion assay with a Matrigel-coated Transwell plate to validate the role of p53 in the effect of muscone. The results showed that the number of migrated cells was significantly elevated in the p53 overexpression and p53 activation groups compared with the muscone treatment group ($P<0.01$) (Fig. 5G).

To further study whether p53 activation is necessary for the modulatory effect of muscone on NP cell senescence, we measured the expression level of critical SASP factors by qPCR; the results showed that p53 activation markedly reversed the downregulation of SASP markers MMP3, MMP13, IL-6 and IL-8 ($P<0.01$), and cell senescence markers $p16^{INK4A}$ and $p21^{CIP}$ ($P<0.05$)caused by muscone in IL-1β-treated NP cells (Fig. 6A,D). Furthermore, these effects were also confirmed at the protein level by Western blotting and quantitative analysis of the data (Fig. 6B,C,E,F). We also performed SA-β-gal staining to validate the role of p53 in the muscone-mediated regulation of the senescence phenotype of NP cells. The results showed that the number of senescent cells was significantly reduced by muscone treatment, as demonstrated by the reduced number of SA-β-gal-positive cells; however, SCH529074 treatment increased the number of senescent cells ($P<0.05$) (Fig. 6G,H).

Next, we explored the role of p53 in muscone's effect on NP cell apoptosis. Since p53 itself is closely related to cell apoptosis, we first measured the expression of *PUMA*, *BAX*, *p21* and *CCNG2*, all of which are known downstream targets of p53 [33,34], and showed that all these targets were downregulated after muscone treatment but upregulated by p53 activation ($P<0.01$) (Fig. 7A). Furthermore, the protein level changes in these genes were confirmed by Western blotting ($P<0.01$) (Fig. 7B). Next, we performed Annexin V-FITC/PI double staining and flow cytometry to assess whether p53 is required for muscone's antiapoptotic effect and showed that p53 overexpression and p53 activation both aggravated apoptosis, while apoptosis was relieved by muscone treatment in the presence of IL-1β ($P<0.01$) (Fig. 7C,D). Moreover, cell cycle analysis confirmed that the acceleration of cell cycle progression in muscone-treated NP cells was inhibited by p53 overexpression or p53 activation ($P<0.01$) (Fig. 7E,F).

Muscone protects against NP degeneration through p53 signaling in vivo

To study the effect of muscone on NP degeneration in vivo, we used a mouse model of needle puncture-induced IDD and injected the mice with muscone or vehicle. The magnetic resonance imaging (MRI) results showed a significant decrease in the T2-weighted signal in the NP between the IDD group and the sham group according to Pfirrmann grade assessment ($P<0.01$) (Fig. 8A). However, muscone treatment protected against the degeneration of the NP in IDD model mice, as indicated by better Pfirrmann grades ($P<0.01$), while p53 activation using SCH529074 reversed the effect of muscone treatment (Fig. 8A). Furthermore, histological analysis by hematoxylin-eosin (HE) staining showed that cells in the NP were obviously replaced by fibrochondrocytes with and that the disc height was reduced in the IDD group; however, muscone treatment protected against NP degeneration, and p53 activation worsened degeneration in the muscone + SCH529074 group ($P<0.01$) (Fig. 8B,D). Moreover, the expression of p53, p21, and p16 was markedly elevated in both the IDD group and muscone + SCH529074 group, but this change was significantly reversed by muscone treatment ($P<0.01$) (Fig. 8C,E–G), implying that muscone protects against NP degeneration and cell senescence through the p53 axis in vivo (Fig. 8H).

Discussion

In our study, we demonstrated that *p53* is a critical mediator of NP cell degeneration and senescence induced by inflammatory factors and that it is closely related to the known NP degeneration-causing factor IL-1β. IL-1β is a classical proinflammatory cytokine that increases the levels of catabolism-related ECM genes, including a disintegrin and metalloproteinase with thrombospondin motifs (ADAMTSs) and MMPs, and decreases the levels of anabolism-related ECM genes, including aggrecan *(ACAN)*, *COL2* and *CHSY1*, in NP tissues. Hence, IL-1β is often applied to induce degeneration and senescence of NP cells in vitro. Gang Gao et al.[35] demonstrated that IL-1β stimulation significantly increases the phosphorylation of p65 and p53 expression. Litao Zhang et al.[36] also indicated that proinflammatory cytokine stimulation obviously increases the expression of p53 and activates the NF-κB/p53 pathway in normal NP cells. Maojie Yang et al.[37] found that treatment with different concentrations of IL-1β elevated the levels of p53 and the downstream gene p21, while these effects could be significantly blocked by Sirtuin 2 overexpression. As expected, the present study indicates that IL-1β notably decreases cell proliferation and the protein/mRNA expression of *ACAN*, *COL2* and *CHSY1* and increases cell apoptosis and the protein/mRNA expression of *ADAMTS4*, *MMP1*, *MMP3* and *MMP13*. We performed mainly used IL-1β to induce NP cell degeneration in vitro; we think it is an appropriate agent for our study because it can induce p53 signaling and produce changes that recapitulate degeneration in vivo.

IDD has been reported to be one of the most common musculoskeletal disorders, and the main feature of IDD is a homeostatic imbalance between anabolism and catabolism in the nucleus pulposus[38]. This homeostatic imbalance in the NP mainly results from proinflammatory factor infiltration, ECM degradation, NP cell apoptosis and cell senescence. The first identified cause of cell senescence is incomplete replication of the ends of DNA, which leads to gradual shortening of telomeres during continuous replication; this mechanism is responsible for the limited replication ability of eukaryotic cells[39]. Previous studies[16,39–42] have demonstrated that *p53* activation by telomere erosion or the DNA damage response (DDR) induces cycle arrest. Upstream factors include cycle checkpoint proteins and DNA repair proteins such as Chk1, Chk2, ATM, and ATR. ATM activates p53 mainly by phosphorylating p53, while ATR activates p53 by phosphorylating CHK1 and CHK2. In the downstream pathway, p53 initiates p21 to inhibit CDK2 to restrain the progression of the cell cycle from G1 to S phase by Rb. Ki-Won Kim et al.[43,44] reported that the levels of *p53* and *p21* are significantly increased, the expression of senescence markers such as SA-β-gal is increased, telomere length is reduced and telomerase activity is decreased in aging NP cells. In addition, the telomere-based p53-p21 pathway plays an important

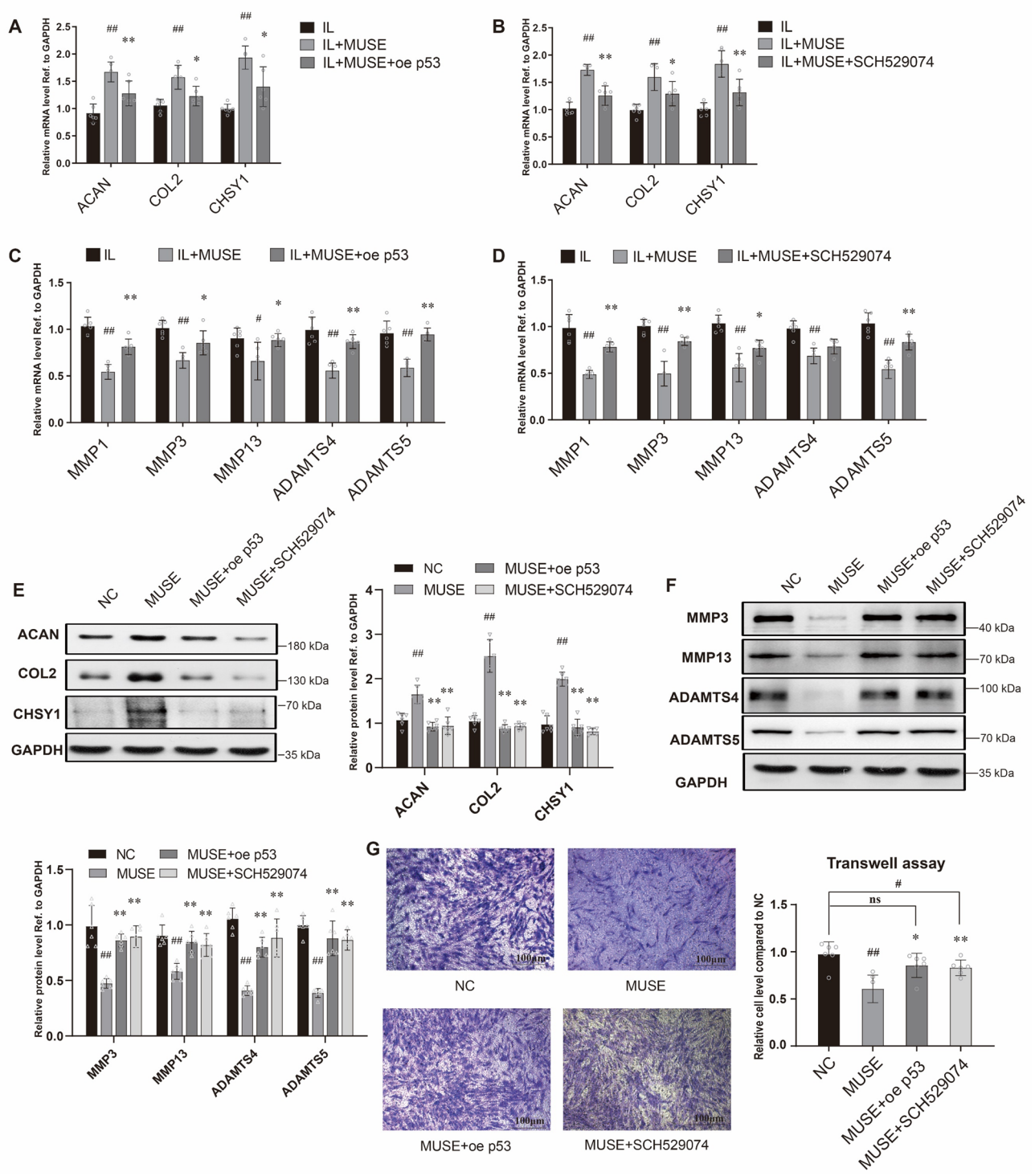

Fig. 5. Muscone attenuates NP cells degeneration via p53 signalling. (**A**,**B**) The mRNA levels of ACAN, CHSY1 and COL2 expression in degenerated NP cell (induced by IL-1β) were measured by qPCR analysis. SCH529074 is the p53 agonist. (**C**,**D**) The mRNA levels of MMP1, MMP3, MMP13, ADAMTS4 and ADAMTS5 expression in degenerated NP cell (induced by IL-1β) were measured by qPCR analysis. (**E**) Western Blot analysis showing the protein levels of ACAN, COL2, CHSY1 and GAPDH expression. (**F**) Western Blot analysis showing the protein levels of MMP9, MMP13, ADAMTS4, ADAMTS5 and GAPDH expression. (**G**) The cell migration in different groups was evaluated by Matrigel coated Transwell invasion assay, bar represents 100 μm. Relative quantitative cell level was evaluated by microscopy and shown in the right panel. NC was used as a control. All experiments were repeated at least 3 times. and GAPDH is used as an internal control in qPCR analysis. Data are shown as mean ± SD. *, $P < 0.05$; **, $P < 0.01$.

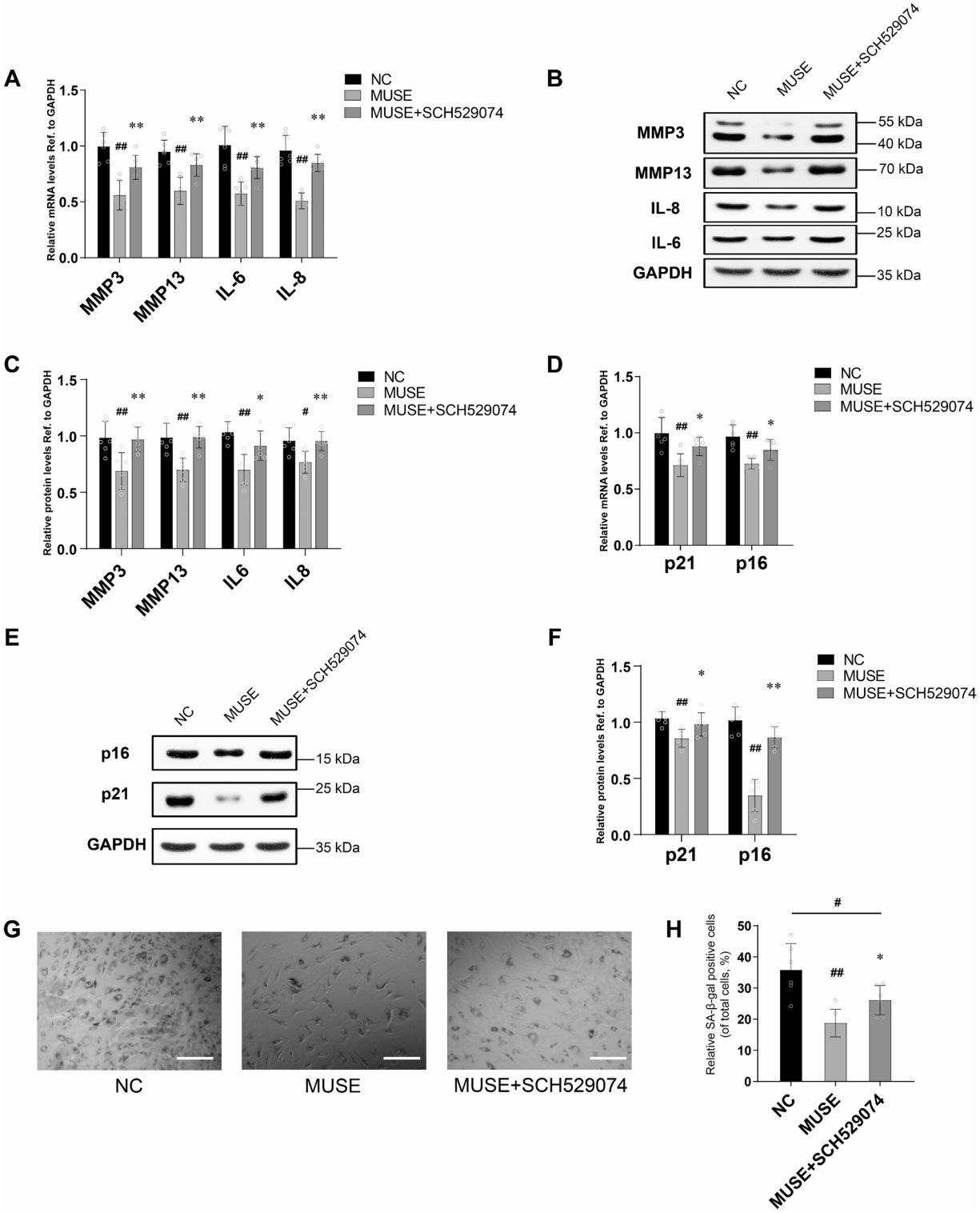

Fig. 6. Muscone alleviates cell senescence and SASP phenotype in NP cells via p53 signalling. (**A**) qPCR analysis showing the relative mRNA expression level of SASP factors, such as MMP13, MMP3, IL-6 and IL-8, in the NP cells, treat with or without SCH529074. (**B**,**C**) Western Blot analysis showing the protein levels of SASP factors in each group. (**D**) The relative mRNA level of p16INK4A and p21CIP expression was detected by qPCR in the NP cells. (**E**,**F**) Western Blot analysis showing the protein levels of p16INK4A and p21CIP in each group. (**G**) SA-b-gal staining was detected, and positive cells were quantified in (**H**), bar represents 200 μm. All experiments were repeated at least 3 times, and GAPDH is used as an internal control. Data are shown as mean ± SD. #, $P < 0.05$; ##, $P < 0.01$.*, $P < 0.05$; **, $P < 0.01$. ##represented vs. NC group, **represented vs. IL group.

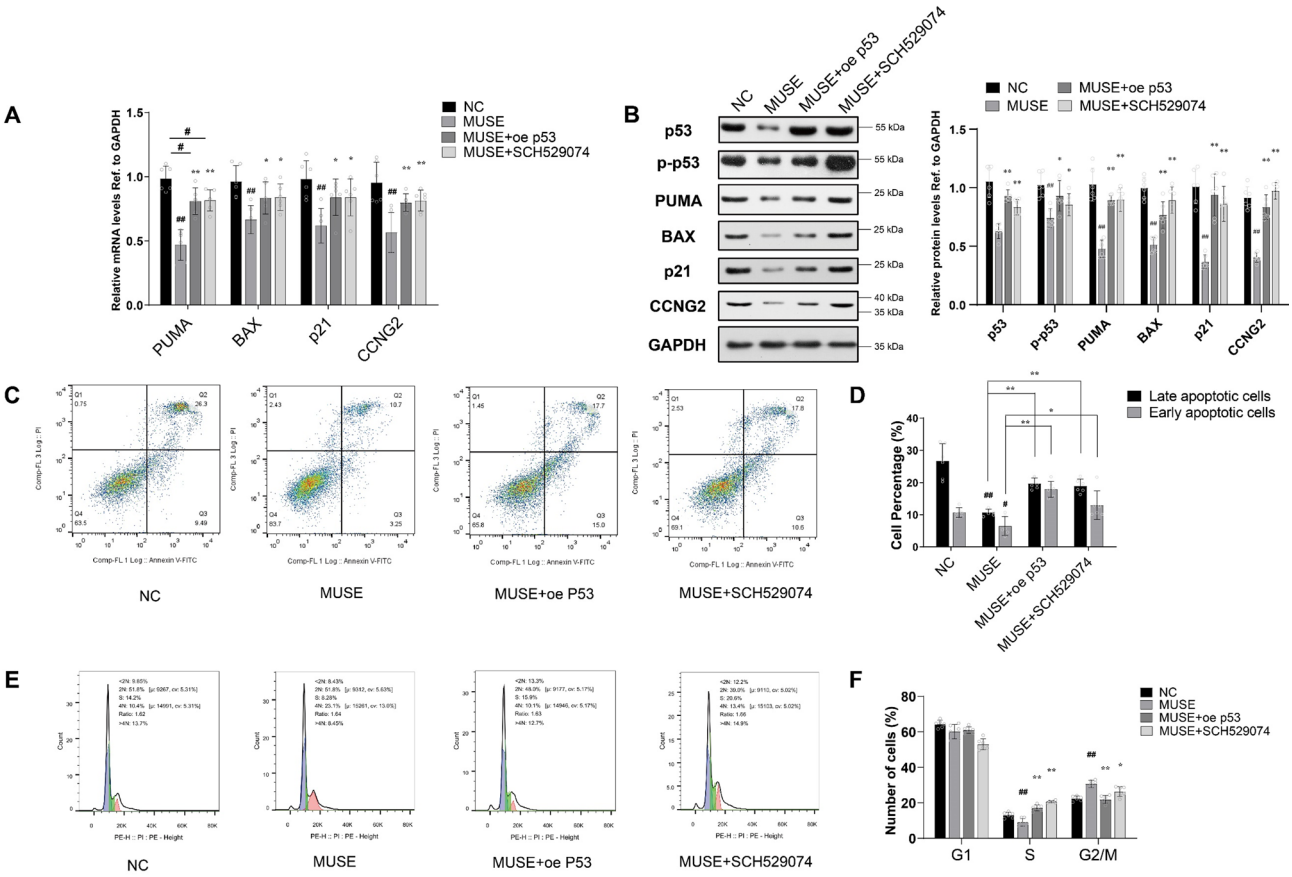

Fig. 7. Muscone attenuates the cell apoptosis of NP cells via p53 signalling. (**A**) qPCR analysis showing the mRNA levels of PUMA, BAX, p21 and CCNG2 expression after p53 overexpression or p53 activation treatment in degenerated NP cell induced by IL-1β. (**B**) The Western Blot analysis showing the protein level changes of PUMA, BAX, p21, CCNG2 and GAPDH expression according to (**A**). (**C**) Annexin V-FITC/PI Double-staining apoptosis assay showing the percentage of apoptotic cell percentage of NP cells under p53 overexpression or p53 activation treatment. (**D**) The mean percentage of early apoptotic cells and late apoptotic cells in each group was shown in the right panel. (**E**) The flow cytometry showing the cell cycle of NP cells under p53 overexpression or p53 activation treatment. (**F**) The number of cells in different cell cycle under different treatment were shown in the panel. All experiments were repeated at least 3 times, and GAPDH is used as an in-ternal control. #, $P<0.05$; ##, $P<0.01$.*, $P<0.05$; **, $P<0.01$. ##represented vs. NC group, **represented vs. MUSE group.

role in the aging and degeneration of NP cells. Jerry E Chipuk et al.[45,46] found that *p53* not only decreases mitochondrial membrane permeabilization and apoptosis by activating the downstream target BAX but also increases nuclear and cytoplasmic levels of pro-apoptotic factors by activating the downstream target *PUMA*. In our study, we found that the levels of p21, BAX and PUMA were elevated by activated p53 in degenerated NP cells, and this effect could be alleviated by muscone treatment.

Muscone, as the key component of musk, is widely applied for the treatment of cardiovascular diseases, cancer, musculoskeletal disorders, neurological disorders and so on. This is because muscone has various pharmaceutical effects, mainly including antiapoptotic and anti-inflammatory effects. Ming-Chao He et al.[47] found that muscone could inhibit LPS-induced neuroinflammation via the NLRP3 inflammasome in the prefrontal cortex. Wen-Xiu Yuan et al.[48] indicated that muscone increased cell proliferation and adipogenic differentiation and reduced osteogenic differentiation via the Wnt/β-catenin signaling pathway in gingival mesenchymal stem cells. Hung Manh Phung et al.[34] demonstrated that muscone protected against renal toxicity by targeting *p53* and the downstream protein *BAX* to decrease ROS levels and exert anti-inflammatory and antiapoptotic effects. However, the molecular mechanism underlying the effect of muscone, especially in the treatment of IDD, is far from fully understood. In our study, muscone significantly blocked the effect of IL-1β in normal NP cells. Different concentrations of muscone can increase the levels of matrix-related genes, including *ACAN*, *CHSY1* and *COL2*, and decrease the levels of inflammation-related genes, including *MMP1*, *MMP3*, *MMP13* and *ADAMTS4*. In addition, both a p53 overexpression plasmid and an activator of *p53* greatly reversed the effect of muscone, which demonstrated that *p53* is indeed a potential downstream target of muscone in an NP degeneration model.

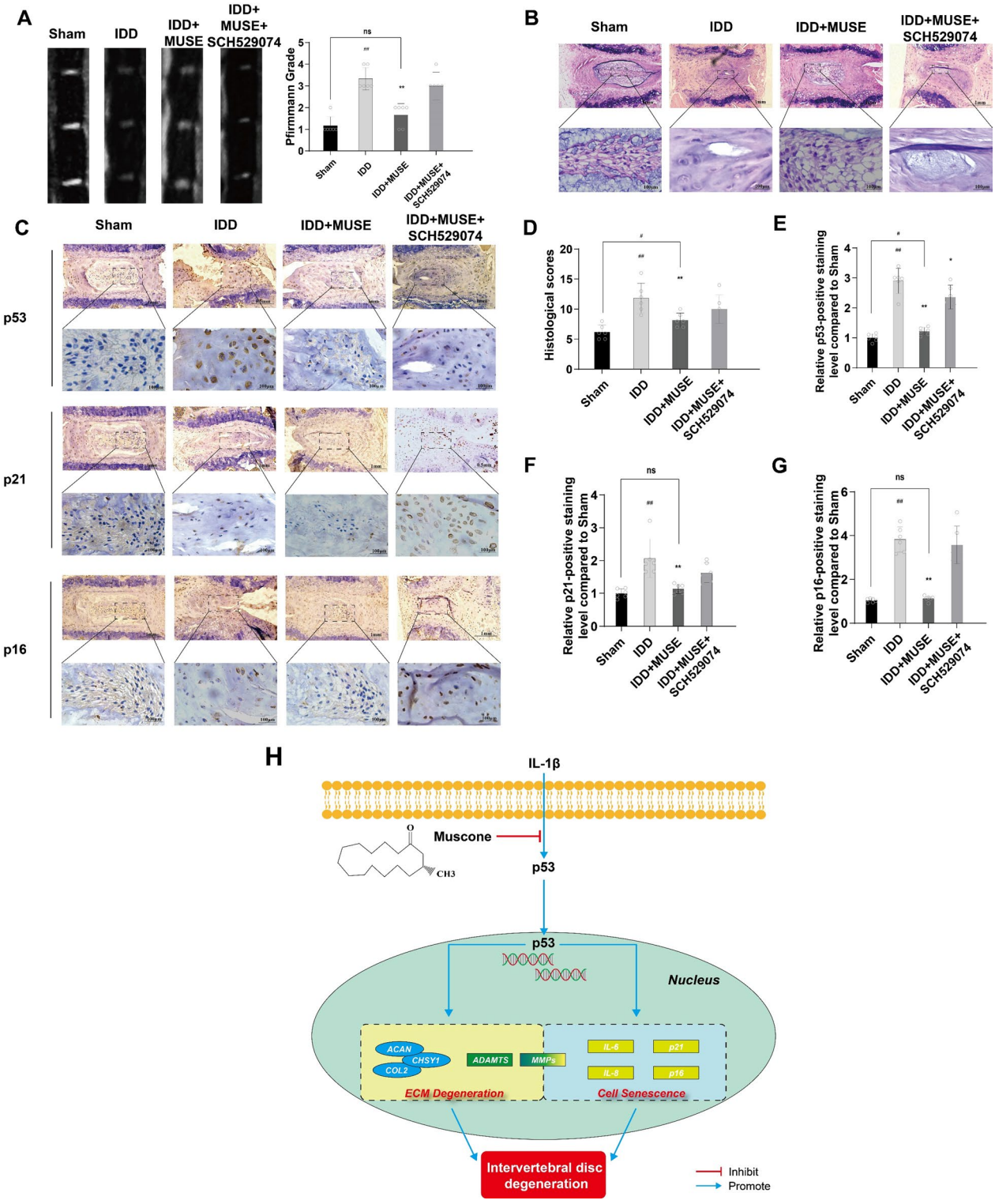

Fig. 8. Muscone alleviates IDD progress through p53 signaling in vivo. (**A**) MRI of the intervertebral disc in mice from the different groups (sham group, IDD group, IDD + muscone group and IDD + muscone + SCH529074 group). Relative Pfirrmann grade score was evaluated and shown in the right panel. (**B**) The HE staining of the intervertebral disc from each group. (**C**) The immuno-histochemical staining assay for p53, p16INK4A and p21CIP in the NP tissue from each group. (**D**) Histological scores of intervertebral disc tissues in each group in (**B**). Quantitative analysis of the proportion of p53- (**E**), p21- (**F**), and p16- (**G**) positive cells in the immunohistochemical staining in (**C**). (**H**) Summery on the mechanism of muscone in intervertebral disc degeneration. Bars represent 100 μm or 1 mm as indicated. Data are shown as mean ± SD. #, $P < 0.05$; ##, $P < 0.01$.*, $P < 0.05$; **, $P < 0.01$. ##represented vs. Sham group, **represented vs. IDD group.

There are some limitations in our study. First, because of the wide effect of muscone on many diseases in vivo, which makes it difficult to investigate the mechanism underlying the effect of this drug in NP tissues, we only examined the effect and mechanism in vitro. In addition, the interaction between muscone and *p53* needs to be further studied in NP tissues. Finally, the effect of oral administration of muscone in vivo needs to be studied deeply. This is an appropriate topic for further study that will be investigated in our future work.

Conclusions

In summary, our data showed that a suitable concentration of muscone prevented degeneration, while an excessive concentration of muscone did not have an ideal effect; this may have been because muscone was diluted with DMSO. Moreover, muscone protected against IL-1β-induced inflammation, apoptosis, senescence and cycle arrest in NP cells by alleviating the phosphorylation of p53 (Fig. 8F). These effects may be mediated through inhibiting expression of the downstream factors *p21*, *Bax* and *PUMA*. Thus, we provide various pieces of evidence that muscone, a natural component of musk, may have potential therapeutic value for IDD, but this requires further investigation.

Data availability

The datasets generated during the current study are available in the Gene Expression Omnibus (GEO) repository (GSE113633), and processed data can be found in supplementary dataset files online. All data used to support the findings of this study are available from the corresponding author Prof. Chen Xu upon reasonable request.

Received: 30 December 2024; Accepted: 11 August 2025
Published online: 14 August 2025

References

1. Chen, S. et al. Global, regional and National burden of low back pain 1990–2019: A systematic analysis of the global burden of disease study 2019. *J. Orthop. Translat*. **32**, 49–58. https://doi.org/10.1016/j.jot.2021.07.005 (2022).
2. Zhong, H. et al. SERPINA1 is a hub gene associated with intervertebral disc degeneration grade and affects the nucleus pulposus cell phenotype through the ADIRF-AS1/miR-214-3p axis. *Transl. Res. J. Lab. Clin. Med*. https://doi.org/10.1016/j.trsl.2022.02.006 (2022).
3. Gao, B. et al. Discovery and application of postnatal nucleus pulposus progenitors essential for intervertebral disc homeostasis and degeneration. *Adv. Sci. (Weinh)*. e2104888. https://doi.org/10.1002/advs.202104888 (2022).
4. Bjornsdottir, G. et al. Rare SLC13A1 variants associate with intervertebral disc disorder highlighting role of sulfate in disc pathology. *Nat. Commun.* **13**, 634. https://doi.org/10.1038/s41467-022-28167-1 (2022).
5. Wei, L. et al. Chondroitin synthase-3 regulates nucleus pulposus degeneration through actin-induced YAP signaling. *Faseb J.* **34**, 16581–16600. https://doi.org/10.1096/fj.202001021R (2020).
6. Zhang, Y. H. et al. Naringin Inhibits Apoptosis Induced by Cyclic Stretch in Rat Annular Cells and Partially Attenuates Disc Degeneration by Inhibiting the ROS/NF-κB Pathway. *Oxid. Med. Cell. Longev.* 6179444, (2022). https://doi.org/10.1155/2022/6179444 (2022).
7. Zhang, Z. et al. Overexpression of Aquaporin-3 alleviates Hyperosmolarity-Induced nucleus pulposus cell apoptosis via regulating the ERK1/2 pathway. *Pain Res. Manage.* **2022** (1639560). https://doi.org/10.1155/2022/1639560 (2022).
8. Zhao, Y., Xiang, Q., Lin, J., Jiang, S. & Li, W. Oxidative stress in intervertebral disc degeneration: new insights from bioinformatic strategies. *Oxid. Med. Cell. Longev.* **2022** (2239770). https://doi.org/10.1155/2022/2239770 (2022).
9. Kritschil, R., Scott, M., Sowa, G. & Vo, N. Role of autophagy in intervertebral disc degeneration. *J. Cell. Physiol.* **237**, 1266–1284. https://doi.org/10.1002/jcp.30631 (2022).
10. Wang, D. et al. Kukoamine A attenuates lipopolysaccharide-induced apoptosis, extracellular matrix degradation, and inflammation in nucleus pulposus cells by activating the P13K/Akt pathway. *Bioengineered* **13**, 8772–8784. https://doi.org/10.1080/21655979.2022.2051855 (2022).
11. Madhu, V. et al. The mitophagy receptor BNIP3 is critical for the regulation of metabolic homeostasis and mitochondrial function in the nucleus pulposus cells of the intervertebral disc. *Autophagy* **19**, 1821–1843. https://doi.org/10.1080/15548627.2022.2162245 (2023).
12. Shao, Z. et al. Senolytic agent Quercetin ameliorates intervertebral disc degeneration via the Nrf2/NF-κB axis. *Osteoarthr. Cartil.* **29**, 413–422. https://doi.org/10.1016/j.joca.2020.11.006 (2021).
13. Murakami, T., Inagaki, N. & Kondoh, H. Cellular senescence in diabetes mellitus: distinct senotherapeutic strategies for adipose tissue and pancreatic β cells. *Front. Endocrinol.* **13**, 869414. https://doi.org/10.3389/fendo.2022.869414 (2022).
14. Roupakia, E., Markopoulos, G. S. & Kolettas, E. Genes and pathways involved in senescence bypass identified by functional genetic screens. *Mech. Ageing Dev.* **194**, 111432. https://doi.org/10.1016/j.mad.2021.111432 (2021).
15. Astrike-Davis, E. M., Coryell, P. & Loeser, R. F. Targeting cellular senescence as a novel treatment for osteoarthritis. *Curr. Opin. Pharmacol.* **64**, 102213. https://doi.org/10.1016/j.coph.2022.102213 (2022).
16. He, Y. et al. Cellular senescence in sarcopenia: possible mechanisms and therapeutic potential. *Front. Cell. Dev. Biology*. **9** https://doi.org/10.3389/fcell.2021.793088 (2021).
17. Kumari, R. & Jat, P. Mechanisms of cellular senescence: cell cycle arrest and senescence associated secretory phenotype. *Front. Cell. Dev. Biology*. **9**, 645593. https://doi.org/10.3389/fcell.2021.645593 (2021).
18. Abdelmohsen, K. & Gorospe, M. Noncoding RNA control of cellular senescence. *Wiley Interdisciplinary Reviews RNA*. **6**, 615–629. https://doi.org/10.1002/wrna.1297 (2015).
19. Ding, M. et al. From non-targeted to targeted GC-MS metabolomics strategy for identification of TCM preparations containing natural and artificial musk. *Chin. Med.* **17** https://doi.org/10.1186/s13020-022-00594-8 (2022).
20. Lv, S. et al. Chemical compositions and Pharmacological activities of natural musk (Moschus) and artificial musk: A review. *J. Ethnopharmacol.* **284**, 114799. https://doi.org/10.1016/j.jep.2021.114799 (2022).
21. Liu, K. et al. Zoology, chemical composition, pharmacology, quality control and future perspective of musk (Moschus): a review. *Chin. Med.* **16**, 46. https://doi.org/10.1186/s13020-021-00457-8 (2021).
22. Yang, L. Q. et al. Muscone derivative ZM-32 inhibits breast tumor angiogenesis by suppressing HuR-mediated VEGF and MMP9 expression. *Biomed. pharmacotherapy = Biomedecine Pharmacotherapie*. **136**, 111265. https://doi.org/10.1016/j.biopha.2021.111265 (2021).
23. Wei, C. J., Hua, F., Chen, Y. H., Zhang, Z. W. & Shen, Z. Y. Muscone alleviates myocardial ischemia-reperfusion injury via Inhibition of oxidative stress and enhancement of SIRT3. *J. Biol. Regul. Homeost. Agents*. **35**, 85–96. https://doi.org/10.23812/20-101-A (2021).

24. Liang, Q. Q., Zhang, M., Zhou, Q., Shi, Q. & Wang, Y. J. Muscone protects vertebral end-plate degeneration by antiinflammatory property. *Clin. Orthop. Relat. Res.* **468**, 1600–1610. https://doi.org/10.1007/s11999-009-1079-0 (2010).
25. Tu, J. et al. Single-Cell transcriptome profiling reveals multicellular ecosystem of nucleus pulposus during degeneration progression. *Adv. Sci. (Weinh).* **9**, e2103631. https://doi.org/10.1002/advs.202103631 (2022).
26. Hu, B. et al. TGF-β induces Up-Regulation of chondroitin sulfate synthase 1 (CHSY1) in nucleus pulposus cells through MAPK signaling. *Cell. Physiol. Biochem.* **37**, 793–804. https://doi.org/10.1159/000430396 (2015).
27. Wang, R. et al. Inflammatory-sensitive CHI3L1 protects nucleus pulposus via AKT3 signaling during intervertebral disc degeneration. *Faseb J.* **34**, 3554–3569. https://doi.org/10.1096/fj.201902096R (2020).
28. Zheng, G. et al. TFEB protects nucleus pulposus cells against apoptosis and senescence via restoring autophagic flux. *Osteoarthr. Cartil.* **27**, 347–357. https://doi.org/10.1016/j.joca.2018.10.011 (2019).
29. Pai, Y. H. et al. Piezoelectric-Augmented thermoelectric ionogels for Self-Powered multimodal medical sensors. *Adv. Mater.* **37**, e2414663. https://doi.org/10.1002/adma.202414663 (2025).
30. Qu, H. et al. Spine system changes in soldiers after load carriage training in a plateau environment: a prediction model research. *Mil Med. Res.* **7** https://doi.org/10.1186/s40779-020-00293-1 (2020).
31. Han, B. et al. A simple disc degeneration model induced by percutaneous needle puncture in the rat tail. *Spine* **33**, 1925–1934. https://doi.org/10.1097/BRS.0b013e31817c64a9 (2008).
32. Fafián-Labora, J. A. & O'Loghlen, A. Classical and nonclassical intercellular communication in senescence and ageing. *Trends Cell Biol.* **30**, 628–639. https://doi.org/10.1016/j.tcb.2020.05.003 (2020).
33. Nenkov, M. et al. Growth inhibitory role of the p53 activator SCH 529074 in non–small cell lung cancer cells expressing mutant p53. *Oncol. Rep.* **43**, 2073–2082. https://doi.org/10.3892/or.2020.7546 (2020).
34. Phung, H. M., Lee, S., Hwang, J. H. & Kang, K. S. Preventive effect of muscone against cisplatin nephrotoxicity in LLC-PK1 cells. *Biomolecules* **10** https://doi.org/10.3390/biom10101444 (2020).
35. Gao, G. et al. Naringin protects against Interleukin 1β (IL-1β)-Induced human nucleus pulposus cells degeneration via downregulation nuclear factor kappa B (NF-κB) pathway and p53 expression. *Med. Sci. Monitor: Int. Med. J. Experimental Clin. Res.* **25**, 9963–9972. https://doi.org/10.12659/msm.918597 (2019).
36. Zhang, L. et al. Effects of the NF–κB/p53 signaling pathway on intervertebral disc nucleus pulposus degeneration. *Mol. Med. Rep.* **22**, 1821–1830. https://doi.org/10.3892/mmr.2020.11288 (2020).
37. Yang, M. et al. Sirtuin 2 expression suppresses oxidative stress and senescence of nucleus pulposus cells through Inhibition of the p53/p21 pathway. *Biochem. Biophys. Res. Commun.* **513**, 616–622. https://doi.org/10.1016/j.bbrc.2019.03.200 (2019).
38. Lyu, F. J. et al. Painful intervertebral disc degeneration and inflammation: from laboratory evidence to clinical interventions. *Bone Res.* **9** https://doi.org/10.1038/s41413-020-00125-x (2021).
39. Ohtani, N. The roles and mechanisms of senescence-associated secretory phenotype (SASP): can it be controlled by senolysis? *Inflamm. Regeneration.* **42** https://doi.org/10.1186/s41232-022-00197-8 (2022).
40. Choi, W. & Lee, E. S. Therapeutic targeting of DNA damage response in cancer. *Int. J. Mol. Sci.* **23** https://doi.org/10.3390/ijms23031701 (2022).
41. Gachechiladze, M., Skarda, J., Bouchalova, K., Soltermann, A. & Joerger, M. Predictive and prognostic value of DNA damage response associated kinases in solid tumors. *Front. Oncol.* **10** https://doi.org/10.3389/fonc.2020.581217 (2020).
42. He, Y. et al. Exosomes derived from tendon stem/progenitor cells enhance tendon-bone interface healing after rotator cuff repair in a rat model. *Bioact Mater.* **40**, 484–502. https://doi.org/10.1016/j.bioactmat.2024.06.014 (2024).
43. Kim, K. W., Chung, H. N., Ha, K. Y., Lee, J. S. & Kim, Y. Y. Senescence mechanisms of nucleus pulposus chondrocytes in human intervertebral discs. *Spine Journal: Official J. North. Am. Spine Soc.* **9**, 658–666. https://doi.org/10.1016/j.spinee.2009.04.018 (2009).
44. Jeong, S. W., Lee, J. S. & Kim, K. W. In vitro lifespan and senescence mechanisms of human nucleus pulposus chondrocytes. *Spine Journal: Official J. North. Am. Spine Soc.* **14**, 499–504. https://doi.org/10.1016/j.spinee.2013.06.099 (2014).
45. Chipuk, J. E. et al. Direct activation of Bax by p53 mediates mitochondrial membrane permeabilization and apoptosis. *Sci. (New York N Y).* **303**, 1010–1014. https://doi.org/10.1126/science.1092734 (2004).
46. Chipuk, J. E., Bouchier-Hayes, L., Kuwana, T., Newmeyer, D. D. & Green, D. R. PUMA couples the nuclear and cytoplasmic proapoptotic function of p53. *Sci. (New York N Y).* **309**, 1732–1735. https://doi.org/10.1126/science.1114297 (2005).
47. He, M. C. et al. Muscone ameliorates LPS-Induced Depressive-Like behaviors and inhibits neuroinflammation in prefrontal cortex of mice. *Am. J. Chin. Med.* **48**, 559–577. https://doi.org/10.1142/S0192415X20500287 (2020).
48. Yuan, W. X. et al. Muscone promotes the adipogenic differentiation of human gingival mesenchymal stem cells by inhibiting the Wnt/β-Catenin signaling pathway. *Drug. Des. Devel. Ther.* **13**, 3291–3306. https://doi.org/10.2147/dddt.S220970 (2019).

Acknowledgements

The authors would like to thank the anonymous reviewers for taking the time and effort to review and ultimately improve the manuscript.

Author contributions

R.W.: Conceptualization, Data curation, Investigation, Resources, Writing - original draft. J.X.: Formal analysis, Investigation, Methodology, Writing - original draft. Z.Z.: Data curation, Formal analysis, Writing - original draft. Y.T.: Data curation, Methodology, Validation. H.Z.: Data curation, Methodology. G.W.: Formal analysis, Validation. L.W.: Investigation, Software. H.W.: Formal analysis, Methodology. X.S.: Resources, Writing - original draft. Y.C.: Data curation, Investigation. P.C.: Resources, Formal analysis. Y.L.: Investigation, Methodology. H.C.: Resources, Validation, Writing - original draft. W.M.: Data curation, Supervision, Validation. W.Y.: Conceptualization, Project administration, Supervision. C.X.: Conceptualization, Supervision, Writing - review & editing.

Funding

This research was supported by grants from the National Natural Science Foundation of China (82172470, 82072469, 82072471, 81972088), Shanghai Municipal Commission of Health and Family Planning Program Excellent academic leader project (2022XD009), Shanghai Education Development Foundation and Shanghai Municipal Education Commission Research and Innovation Program Major project (2023ZKZD45), Shanghai Science & Technology Commission Excellent academic leader project (21XD1404800) and Biopharmaceutical science and technology supporting foundation (21S31901400).

Declarations

Competing interests
The authors declare no competing interests.

Ethics approval and consent to participate
Ethics approval and informed consent was approved by the ethics committee of Shanghai Changzheng Hospital (2021SL044). Informed consent was provided by the patients and their relatives before harvesting intervertebral disc tissue during surgery. All animal experiments were performed in accordance with ARRIVE guidelines, and were approved by the Institutional Animal Care and Use Committee of Second Military Medical University.

Patient consent for publication
Not applicable.

Additional information
Supplementary Information The online version contains supplementary material available at https://doi.org/10.1038/s41598-025-15811-1.

Correspondence and requests for materials should be addressed to H.C., C.X., W.M. or W.Y.

Reprints and permissions information is available at www.nature.com/reprints.

Publisher's note Springer Nature remains neutral with regard to jurisdictional claims in published maps and institutional affiliations.